The effects of amidophosphonate ligand immobilization method on the uranium extraction efficiency of functionalized silica

Aline Dressler, Tom Le Nedelec, Antoine Leydier, Frederic Cuer, Thomas Dumas, Agnès Grandjean

Chemical Engineering Journal Advances 9 (2022) 100225

Contents lists available at ScienceDirect

Chemical Engineering Journal Advances

journal homepage: www.sciencedirect.com/journal/chemical-engineering-journal-advances

The effects of amidophosphonate ligand immobilization method on the uranium extraction efficiency of functionalized silica

Aline Dressler, Tom Le Nedelec, Antoine Leydier *, Frederic Cuer, Thomas Dumas, Agnès Grandjean

CEA, DES, ISEC, DMRC, CEA Marcoule, Commissariat a l'Energie Atomique et aux Energies Alternatives Marcoule, Université Montpellier, Centre De Marcoule, Bagnols sur Cèze 30207, France

ARTICLE INFO

Keywords:
Functionalized silica
Hybrid material
Uranium
Effluent
Extractionl
Capacity
Selectivity
Sulfate
EXAFS

ABSTRACT

The effects on the uranium extraction efficiency of the functionalization method of three kinds of functionalized silica materials were evaluated in low sulfate (pH = 2) and high sulfate (pH = 1) solutions, with compositions representative of typical effluents from uranium mines and leaching solutions from uranium ore treatment, respectively. Silica supports were functionalized with amidophosphonate moieties either by peptide grafting or by non-covalent impregnation. Prior to impregnation, the surface of the silica supports was modified with either alkyl chains or ionic liquid groups. The selectivity of the modified silica supports for uranium was determined in the presence of iron and molybdenum as competing cations. Our results show that both incorporation methods yield materials with good extraction efficiency and selectivity in low sulfate solutions. EXAFS data indicate that uranyl species have to first be desulfurized to be extracted by the phosphonate ligand. This process appears more energetically favorable for the impregnated ligands than for the grafted ones under high sulfate conditions; likely because the grafted ligands compete less efficiently with the bidentate sulfates coordination in uranyl coordination sphere.

Introduction

Solid phase extraction (SPE) is a particularly attractive process to selectively recover low-concentration uranium from acidic aqueous solutions. Its two main advantages compared with liquid/liquid extraction are that the process is solvent-free and compact, with the possibility of performing extraction and back-extraction in separate locations. For example, ores can be extracted on mining sites and then back-extracted in a purification center after transportation. A well-investigated SPE strategy for the removal of uranium ions from aqueous effluents has been to functionalize metal oxide particles, [1] mesoporous silica [2–4], carbon supports [5–8] or MOFs [9,10] using specific organic complexes and also by photocatalytic reduction of U(VI) [11,12].

Among these, carbamoylalkylphosphonates have been shown to have good liquid-liquid uranium extraction properties in (acidic) phosphate [13,14] and sulfate [15] solutions. These bifunctional amidophosphonate ligands have a high distribution factor for U(VI) extraction and are highly selective versus Fe(III) in acidic solutions [16] both in solvent extraction [17–19] and SPE [20–22].

The efficiency and selectivity of the uranium extraction process depend on a variety of parameters. In liquid-liquid processes, the most important parameters are the nature of the solution (e.g. sulfate or phosphate), the presence of competing cations (Fe and/or Mo for example), and the chemical nature of the ligands and their concentration in the organic phase. In the liquid-liquid extraction of uranium from phosphate or sulfate solutions with carbamoylalkylphosphonates for example, it has been shown that the extraction mechanism depends on the phosphate or sulfate concentration: the more phosphate/sulfate there is in the solution, the higher the ligand-to-uranium ratio has to be for uranium complexation [23].

All these parameters may also affect the efficiency of SPE processes. For example, we maximized uranium extraction from low sulfate acid solutions by adjusting the length and the steric hindrance of the alkyl chain of carbamoylalkylphosphonates grafted onto a silica support [24].

However, the mesostructure of the solid phase and the distribution of the ligand inside the pores are also important. We have shown previously [20] that the uranium extraction capacity and selectivity of silica materials depend on the initial size of the pores into which the organic

* Corresponding author.
E-mail address: antoine.leydier@cea.fr (A. Leydier).

https://doi.org/10.1016/j.ceja.2021.100225

Available online 4 December 2021

structures are grafted.

Whereas in liquid-liquid processes the ligands are fully accessible, this is not the case in SPE where ligand accessibility depends strongly on the arrangement of the organic structures inside the silica pores. The present study investigates how different modes of insertion of the same carbamoylalkylphosphonate ligand into the same mesoporous silica support can be used to obtain various arrangements of the organic moieties in the pores of the support. These arrangements on the surface of the pores are then linked with the uranium extraction efficiency in SPE in terms of extraction capacity (isotherm) and selectivity towards Fe and Mo.

Materials and methods

Material design

Fig. 1 shows how the ligand (Di-2-EthylHexylCarbamoyleEthylButyl Phosphonate, referred to in the following as DEHCEBP) was attached onto the same Davisil 60 (D60) silica support either by grafting via a covalent peptide bond as described by Charlot et al. [20] (grafted@D60) or by impregnation onto D60 prefunctionalized silica with alkyl chains (AdsC8@D60) or with ionic liquid chains (AdsMiMBr@D60).

Effluent solutions

Mining effluents vary in sulfate concentrations and composition. Therefore, two sulfuric acid solutions were selected and compared in this study: a low sulfate, low competing cation (Mo and Fe) uranium solution typical of mine effluents (referred to hereafter as the "low sulfate" solution), and a high sulfate high Fe and Mo solution typical of leaching solutions from uranium ore treatment (referred to hereafter as the "high sulfate" solution). The pH was adjusted using sulfuric acid and the desired $[SO_4]^{2-}$/ [U] ratio was achieved by adding sodium sulfate. For the solutions with competing ions, Fe was added as iron sulfate ($Fe_2(SO_4)_3 \bullet 7H_2O$) and Mo as sodium molybdate (Na_2MoO_4). The initial compositions of the studied solutions are given in Table 1.

The impact of the initial sulfate concentration on the uranium extraction capacities of the studied materials was analyzed using solutions with and without competing ions (Mo and Fe), to separately evaluate the effects of the functionalization method on the uranium extraction capacity and selectivity of the materials.

Table 1
Initial compositions of the studied uranium-containing solutions.

Solution		U (mg/L)	Fe (mg/L)	Mo (mg/L)	pH	$[SO_4]^{2-}$/ [U]
Low	Isotherm	119	-	-	2	50
Sulfate	Selectivity	119	12,5	29,5	2	50
High	Isotherm	400	–	-	1	900
Sulfate	Selectivity	400	5000	57	1	900

Chemicals

All organic reagents were used as received from Aldrich, Acros and Fluka. Solvents were purchased from Acros, Pro-Labo, Fluka, and Aldrich. Anhydrous solvents were obtained from Acros.

Materials synthesis

Di-2-EthylHexylCarbamoylEthylButyl Phosphonate (DEHCEBP) was prepared as described by Turgis et al. [16] The grafted and impregnated materials were synthesized in two steps (Fig. 2). Commercial mesoporous silica supports (Davisil60, Aldrich) were pre-functionalized by direct silanization with either commercial aminopropyltriethoxysilane (APTES), octyltrimethoxysilane or 1-methyl-3- [3-(triethoxysilyl)propyl]imidazolium bromide obtained as described in the literature, [25, 26] respectively yielding NH_2@D60, C8@D60, and MiMBr@D60. Amidophosphonate moieties were then attached. The grafted material (grafted@D60) was prepared by peptide coupling as previously described [27]. The impregnated materials were prepared as follows: 2.5 g of previously prefunctionalized silica (C8@D60 or MiMBr@D60) was mixed with 25 ml of dichloromethane containing 1.2 mmol of DEHCEBP in a 50 mL round bottom flask for 3 h The final materials (AdsC8@D60 and AdsMiMBr@D60) were obtained after evaporation of the solvents and overnight vacuum drying.

Further experimental details and data on the ligand and the prepared materials are provided in the supporting material ("I-ligand" for DEHCEBP and "II-Materials" for the final materials).

Analytical techniques

Solution ^{1}H, ^{31}P and ^{13}C NMR spectra were recorded on a Bruker 400

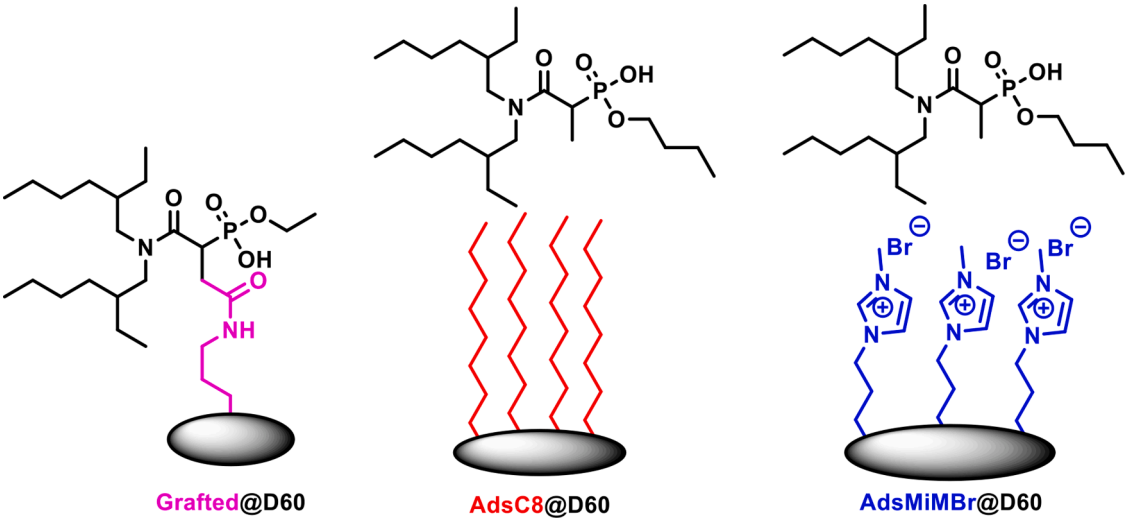

Fig. 1. Schematic diagrams of the studied amidophosphonate materials.

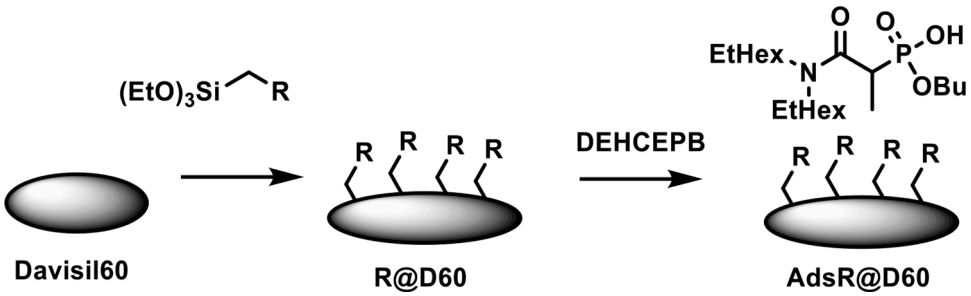

Fig. 2. Schematic summary of the two-step process used to synthesize the studied amidophosphonate materials.

ultrashield VS spectrometer (Larmor frequencies, 400.13 MHz for ^{1}H, 161.976 MHz for ^{31}P, 100.613 MHz for ^{13}C) using deuterated chloroform as the solvent and internal standard. Solid-state cross-polarization magic-angle spinning (CP-MAS) ^{13}C, ^{31}P and ^{29}Si NMR spectra were recorded on a 400 MHz Bruker Avance spectrometer. The samples were spun at 10 kHz. Triphenylphosphine oxide was used as internal standard to quantify the ^{31}P contents of the materials.

Attenuated total reflection (ATR)-FTIR experiments were carried out using a Nicolet iS50 device equipped with an ATR element (a diamond crystal plate). The data obtained were processed using Omnics 9.2 (Thermo Electron Corporation). A background spectrum was recorded prior to each experiment so that the contributions of carbon dioxide, water vapor and diamond crystals to the spectrum could be subtracted. Each spectrum was obtained as an average of 32 scans in the range 400–4000 cm^{-1} at 4 cm^{-1} resolution. ATR corrections were applied during processing.

The uranium, iron and molybdenum concentrations used to calculate the extraction capacity and selectivity of the materials were measured in the extraction experiment solutions by ICP-AES (2% nitric acid; Analytik Jena PlasmaQuant PQ9000).

Nitrogen sorption–desorption isotherms were measured at −196 °C using a Quantachrome Novatouch LX3 surface area and pore size analyzer. Samples were degassed at 90 °C for 24 h prior to analysis. Surface areas were calculated using the Brunauer–Emmett–Teller (BET) method. Pore sizes were taken as the maximum of the corresponding distribution calculated using the Barrett–Joyner–Halenda (BJH) method. Total pore volumes were calculated using the volume of adsorbed gas at P/P_0=1. The nitrogen sorption isotherm and pore size distribution calculated using the BJH method for each support are given in Table S1 in the supporting material.

Ligand concentrations per gram of solid (τ_L, mmol•g^{-1}) were measured by thermogravimetric analysis (TGA; Mettler Toledo), an approach validated by Charlot et al. [20] by comparison with carbon and nitrogen analysis. About 20 mg of material was placed in a 70 µL alumina pan and heated from 303 to 1273 K at 5 K•min^{-1} under 30 mL•min^{-1} air flow. Ligand concentrations were also measured by quantitative ^{31}P NMR. A sealed vial containing a known amount of triphenylphosphine oxide was added as internal standard alongside the sample, and the mass of amidophophonate in the material was determined by comparing the respective integrated intensities of the two ^{31}P NMR signals.

Uranium extraction experiments

Sorption isotherms were measured in the absence of competing ions to determine the maximum extraction capacity of the materials, and extraction selectivity experiments were conducted separately to evaluate the effect of competing cations. For the sorption isotherm experiments, approximately 50 mg of solid was added to a series of flasks, each one containing different volumes of the considered solution. The solid/liquid ratios ($\Psi_{S/L}$, mg•mL^{-1}) ranged from 2 to 10 in the low sulfate solution and from 5 to 50 in the high sulfate solution. The extraction experiments were performed in batch mode at 25 °C under shaking for 24 h after 48 h of conditioning in the absence of uranium. Previous work with the same kind of ligand grafted onto silica with various pore sizes showed that equilibrium was reached within 5 h, meaning that the 24 h extraction time allows to reach equilibrium [20].

To measure the selectivity of the materials in the presence of competing ions, uranium extraction experiments were performed under saturated conditions, as identified from the previous sorption isotherms. The solid/liquid ratios in the low and high sulfate solutions were 2.8 and 5.0, respectively. The extraction experiments were carried out using the same protocol as for measuring the sorption isotherms.

After the extraction experiments, the studied materials were separated from the liquid phase by filtration through a 0.22 µm cellulose acetate membrane. The concentrations of ions in the liquid phase before and after contact with the functionalized solid were measured by ICP-AES. These values were then used to calculate the extraction capacity at equilibrium ($Q_{X,e}$), namely the mass or amount of uranium extracted per gram of solid:

$$Q_{X,e} = \left[X_i - X_{eq}\right] * \frac{V}{m} \quad (1)$$

where X_i and X_{eq} (mg•L^{-1} or mmol•L^{-1}) are the uranium concentrations in the solution respectively before contact and at equilibrium between the solid and the solution, V is the volume of the solution (L) and mis the mass of the solid sample (g).

The measured concentrations of ligand (τ_L, mmol•g^{-1}) inside each solid support were used to determine the required ligand to uranium molar ratio (L/U) for each material:

$$L/U = \frac{\tau_L}{Q_{U,e}} \quad (2)$$

If all ligand molecules are accessible for extraction, L/U gives the stoichiometric coefficients of the complexes formed inside the pores of the material during extraction.

The selectivity factor (SF) of the materials for uranium in the presence of Mo and Fe as competing ions was calculated using Eq. (3):

$$SF_Y^X = \frac{\frac{Q_{X,e}}{Q_{Y,e}}}{\frac{[X]_i}{[Y]_i}} \quad (3)$$

Isotherm modeling

The measured uranium extraction isotherms were fitted with the Langmuir model or the Freundlich model. The Langmuir model is given by:

$$Q_{U,} = \frac{Q_{max} K_l \, [U]_{eq}}{1 + K_l \, [U]_{eq}} \quad (4)$$

with

$$K_l = \frac{\overline{[LU]}}{[U]_{eq}.\overline{[L]}} = \frac{Q_{U,eq}}{\left([U]_{eq}(Q_{max} - Q_{U,eq})\right)} \quad (5)$$

where K_l, the Langmuir constant, is a measure of a material's affinity for the targeted element; $\overline{[LU]}$ is the concentration of ligand-uranium complexes on the surface of the material, $\overline{[L]}$ is the concentration of free ligand, $[U]_f$ (mmol•g^{-1}) is the uranium concentration in the liquid phase after contact with the solid phase (at equilibrium), and Q_{max} and $Q_{U,eq}$ (mmol•g^{-1}) are the maximum and equilibrium uranium extraction capacities.$Q_{U,e}$ was obtained from the experimental data and Eq. (5) can be linearized as follows:

$$\frac{[U]_{eq}}{Q_{U,e}} = \frac{1}{K_l Q_{max}} + \frac{[U]_{eq}}{Q_{max}} \quad (6)$$

The Freundlich model is given by:

$$Q_{U,} = K_n\left([U]_{eq}\right)^{1/n} \quad (7)$$

Where K_n is the Freundlich constant and n a constant.

X-ray absorption spectroscopy

Extended X-Ray absorption fine structure (EXAFS) spectra of the initial high sulfate uranium solution (pH = 1.5) and of the three intermediate (D60, C8@D60, MiMBr@D60) and functionalized (grafted@D60, AdsC8@D60 and AdsMiMBr@D60) materials after contact with this uranium solution were recorded at the MARS beamline of the SOLEIL synchrotron (Saint-Aubin, France) at 2.75 GeV and 450 mA. This beamline is equipped with a water cooled Si(220) double crystal horizontal focusing monochromator. A 13-element HPGe solid-state detector (ORTEC) was used to collect the data in fluorescence mode. The monochromator was energy-calibrated using the yttrium K edge at 1,117,038 eV for uranium measurements. All measurements were performed at room temperature in 200 μL double-layered cells specifically designed for radioactive samples.

The data were processed with the ATHENA code [28]. After energy calibration, the E_0 value was set to the maximum of the uranium absorption edge (17.177 keV). The EXAFS signal was extracted by subtracting a linear pre-edge background and a combination of cubic spline functions for the atomic absorption background; the data were then normalized using the Lengeler–Eisenberg method. The pseudoradial distribution functions were obtained by Fourier transform in $k^3\chi(k)$ with ATHENA [28] between 3.5 and 13.4 Å^{-1} for uranium. The fit quality is determined using *R*-factor and reduced χ^2 both calculated with the ARTEMIS module [28].

The back-scattering amplitude and the phase-shift function were obtained from FEFF 8.4 calculations [29] performed on model structures. At the uranium L_{III} edge, the fitting operations were all performed in *R*-space over individual radial distances for the three first-shell scattering paths and the two second-shell scattering paths. U-O_{yl} multiple scattering path were also included with parameters constrained as twice the values of the corresponding single spattering path. In one hand the Debye–Waller factors for the four longer coordination shell (σ^2_{Os}, σ^2_{Ol}, σ^2_{L1}, σ^2_{L2}) were constrained to previously reported values. This was decided to allow a reliable comparison between coordination numbers (CN) for each sample and limit correlation between σ^2, CN and S_0^2. In another hand, for the main contribution from the O_{yl} short bonds it is the coordination numbers that is set to 2 because the uranyl structure is known to be very rigid. It allows both the σ^2_{Oyl} and S_0^2 to be considered as floating parameters [22].

Results and discussion

Structural characterization

During prefunctionalization (with amino groups for the grafted material, alkyl chains or ionic liquid groups for the impregnated materials), the silane groups attach to the surface of the silica support via one R-Si(OSi)(OR')$_2$ bond (T1 mode, *R* = 3-aminopropyl, Octyl or 3-BrMiMpropyl, R' = hydrogen or an ethoxy group), two R-Si(OSi)$_2$(OR') bonds (T2 mode), or three R-Si(OSi)$_3$ bonds (T3 mode). We have previously presented ^{29}Si solid-state NMR spectra of these materials [24] that show that the organic moieties are mainly linked to the silica surface in T2 mode—implying the presence of silica-linked ethoxy groups—and in T3 mode [30]. The same results were obtained in the present study (Supporting Material† II Materials). The attachment of the desired organic groups (aromatics for MiMBr@D60, alkyls for NH_2@D60 and C8@D60) was also confirmed by ^{13}C solid state NMR, with the observation of peaks assigned to carbamoylalkylphosphonates as well.

The peak at 1644 cm^{-1} ($\nu_{P\text{-}OH}$, phosphonate) observed in the FTIR spectra of all three materials (Fig. 3) confirms the presence of the ligand inside the materials. The IR band at 3150–3088 cm^{-1} ($\nu_{=C-H}$, aromatic imidazole), only found in the spectrum of AdsBrMIM@D60, confirms the presence of the ionic liquid moiety, while the IR band at 1550 cm^{-1} ($\nu_{C=O}$, amide) found only in the spectrum of the grafted@D60 material confirms, alongside the NMR data, that the carbamoylphosphonate molecules are anchored to the silica surface.

The nitrogen adsorption isotherms recorded for the materials (Fig. 4) show that the volume of adsorbed gas decreases as the materials are functionalized, consistent with the immobilization of organic species on the surface of the pores of the silica support, whose concentrations were measured by ^{31}P NMR (Table 2). These data allow the volume occupied by the ligand inside the materials (L/DV_{ads}) to be calculated using Eq. (8).

$$L/DV_{ads} = \tau_L/((V_{adsMax}Step1) - (V_{adsMax}Step2)) \quad (8)$$

where V_{adsMax} corresponds to the volume at $P = P_0$ in the nitrogen adsorption isotherms.

The concentration of ligand in the grafted@D60 material (0.29 mmol•g^{-1}) measured here by ^{31}P NMR is in agreement with the value measured previously using the same approach [20] confirming the reproducibility of the method. The concentrations of ligands in the impregnated materials were slightly higher: 0.32 mmol•g^{-1} in AdsC8@D60 and 0.34 mmol/g in AdsMiMBr@D60. Since the added amidophosphonates moieties are similar, they should occupy similar volumes inside the pores and indeed, similar [L]/ Vads values were obtained for the three materials.

The purity of the ligands immobilized on the supports after the second synthesis step was monitored by ^{31}P solid state NMR (Fig. 5). A single signal was observed for the grafted material, as we previously reported, proving amongst other spectra that the material was correctly functionalized. Following a similar behavior, impregnated samples tend to have a single singlet around 26 ppm on the ^{31}P NMR spectrum.

Extraction of uranium from sulfuric acid solutions

Speciation studies have shown that in sulfate solutions, uranium is present as uranyl monosulfate $UO_2(SO_4)_{(aq)}$, disulfate $UO_2(SO_4)_2^{2-}$ and potentially as trisulfate $UO_2(SO_4)_3^{4-}$ groups [31,32]. Since both the solutions studied here had low pH and sulfate was in excess, the predominant species was uranyl disulfate $UO_2(SO_4)_2^{2-}$ with mono- or bidentate coordination, the former predominating at low sulfate-to-uranyl ($[SO_4]^{2-}$/ [U]) ratios and the latter predominating at high sulfate-to-uranyl ratios [31]. The complexes formed are $UO_2(SO_4)_2(H_2O)_n^{2-}$ with n varying from 3 to 1 depending on the sulfate concentration [31].

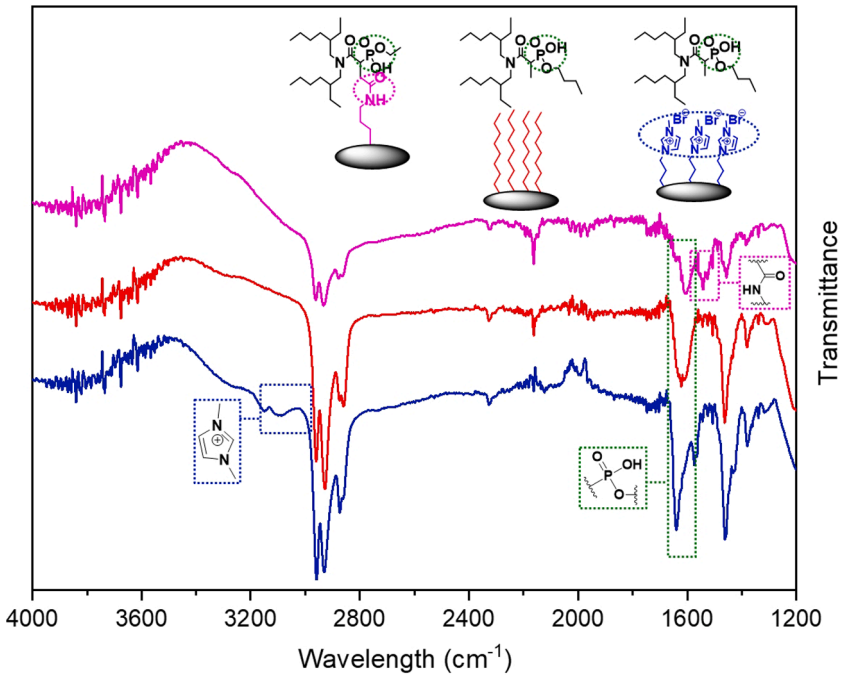

Fig. 3. Fourier-transform infrared spectra with corresponding schematic representations of the three studied materials.

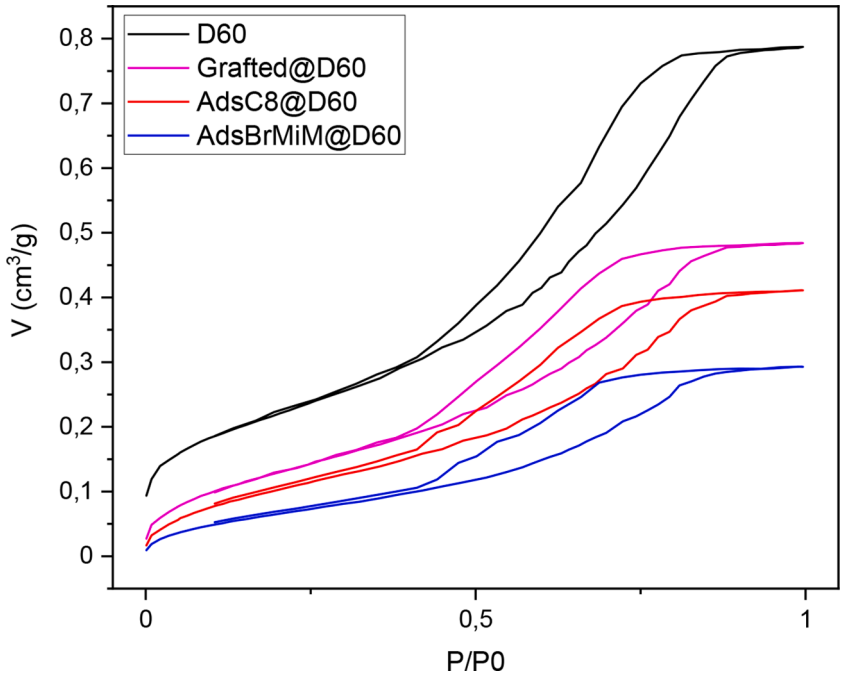

Fig. 4. Nitrogen adsorption isotherms of the three studied materials and of the initial Davisil 60 silica support.

Table 3 summarizes the results obtained from extraction experiments under saturated conditions performed with the non-functionalized "intermediate" materials to discriminate the effects of the different groups (silanol, amino, alkyl, and MiMBr groups) present on the surface of the pores.

In the low sulfate solution, the only material that extracted detectable quantities of uranium was NH_2@D60, indicating that under these conditions, of the different surface species, only amino groups extract uranium, as reported previously [20]. The extraction capacity of the amino groups is very low moreover, less than 10% of the total capacity of the final material (see below). In the presence of competing cations, the only detectable extraction capacities were for Mo with the materials NH_2@D60 and MiMBr@D60, with very low values in both cases (Table 3).

In the high sulfate solution, none of the three "intermediate" materials extracted any U, Fe or Mo from the solution, meaning that the uranium extraction capacities of the functionalized materials are exclusively due to the amidophosphonate ligands.

Uranium extraction from a low sulfate solution

As observed previously for the grafted material [20], Fig. 6a shows

Table 2
Adsorption properties and ligand concentrations in the prefunctionalized and final materials.

Material	S_{BET} ($m^2 \bullet g^{-1}$)	V_{adsMAX} ($cm^3 \bullet g^{-1}$)	τ_L ($mmol \bullet g^{-1}$)	$L/\Delta V_{ads}$ ($mmol \bullet cm^{-3}$)
D60	520 (±16)	0.79 (±0.02)	–	–
NH_2@D60	374 (±11)	0.63 (±0.02)	0.83 (±0.04) (TGA)	–
Grafted@D60	336 (±10)	0.48 (±0.01)	0.29 (±0.01) (^{31}P NMR)	1.00 (±0.06)
C8@D60	409 (±12)	0.67 (±0.02)	0.73(±0.04) (TGA)	–
AdsC8@D60	274 (±8)	0.41 (±0.02)	0.32 (±0.01) (^{31}P NMR)	1.07(±0.06)
MiMBr@D60	353 (±11)	0.66 (±0.02)	0.15 (±0.01) (TGA)	–
AdsMiMBr@D60	176 (±5)	0.29 (±0.01)	0.34 (±0.01) (^{31}P NMR)	1.02(±0.06)

that all three materials have a good affinity for uranium in the low sulfate solution; the extraction capacity increases rapidly before leveling off at 30–40 $mg \bullet g^{-1}$ once the equilibrium concentration is reached. The data are well fit by Langmuir isotherms ($R^2 > 0.99$, Table 4). Based on the Langmuir constants (K_l) of the three materials, these results suggest that the most selective for uranium is AdsMiMBr@D60, and the least selective is grafted@D60.

Fig. 6b shows the ligand-to-uranium ratios obtained from these data. At equilibrium in the grafted material (in the absence of competing ions) only about 2.4 ligand molecules are required to extract each uranyl ion, in agreement with previous results [22], suggesting that under these pH and sulfate conditions, the uranyl equatorial plane consists of two ligands bonded in monodentate fashion via a phosphonate group, two monodentate sulfate groups and a water molecule.

For AdsC8@D60, Fig. 6b shows that on average, roughly 2.7 ligand molecules are required to extract one uranyl ion. This ratio is similar to the grafted material's considering that the remaining amino groups on the surface can also extract a little uranium in this medium, as shown above (Table 3). The ligand/uranium ratio for AdsMiMBr@D60 at equilibrium is slightly lower, at about 2.0, suggesting that the ionic liquid moieties facilitate the migration of uranyl groups into the organic layer and/or arrange the amidophopshonate moieties in such a way as to promote the formation of complexes with uranium. This result is consistent with the higher uranium affinity of this material suggested by the extraction isotherms (Fig. 6a).

Fig. 7. shows the selectivity factors calculated using the extraction capacities measured for U, Fe and Mo.

Selectivity factors greater than 1 mean that the material is selective for uranium over Fe and Mo whereas values less than 1 mean that the material has a higher affinity for the competing ion. In agreement with the Langmuir modeling results, Fig. 7 shows that the grafted material is the least selective. Regarding the selectivity for uranium versus iron and molybdenum, it seems that the functionalization method only has a minor effect on the extraction mechanisms for these competing ions, but that the impregnated materials are the most selective.

Uranium extraction from a high sulfate solution

In the high-sulfate solution and in the absence of competing cations, the results obtained (Fig. 8) suggest that the mode of attachment of the amidophosphonate moieties on the surface of the pores in the silica support has a greater effect than in the low sulfate solution. At equilibrium, roughly 2.6 ligand molecules are required per uranyl ion in the grafted material, compared with about 2.1 in the two impregnated materials. Langmuir Model does not describe the sorption isotherm of the grafted material as well as the ones obtained with the impregnated materials. The Freundlich model show a better fit to describe the behavior of the grafted material ($R^2 = 0.9875$), suggesting a more

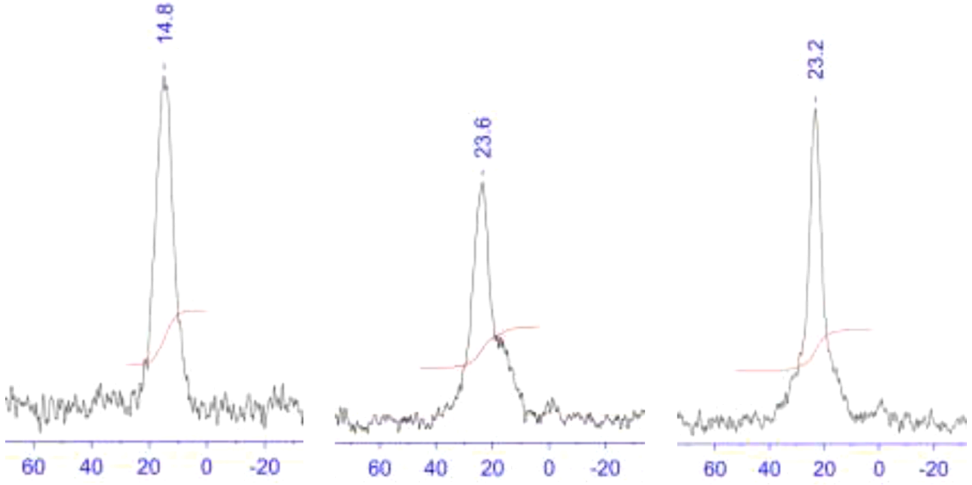

Fig. 5. Magic-angle spinning ^{31}P NMR spectra of grafted@D60 (left), AdsC8@D60 (center) and AdsMiMBr@D60 (right) (Larmor frequency 161.976 MHz for ^{31}P).

Table 3
Extraction capacities of the studied materials before functionalization with amido-phosphonate ligands.

Material	Low Sulfate solution Isotherm solution (U)	Selectivity solution (U, Fe, Mo)			High Sulfate solution Isotherm solution (U)	Selectivity solution (U, Fe, Mo)		
	Q_U	Q_U	Q_{Fe}	Q_{Mo}	Q_U	Q_U	Q_{Fe}	Q_{Mo}
C_8@D60	0*	0*	0*	0*	0*	0*	0*	0*
MiMBr@D60	0*	0*	0*	1.6 ± 0.1	0*	0*	0*	0*
NH_2@D60	3.2 ± 1.4	1.7 ± 1.4	0*	1.7 ± 0.3	0*	0*	0*	0*

Extraction capacities in $mg \bullet g^{-1}$.
* Below ICP-AES detection limit.

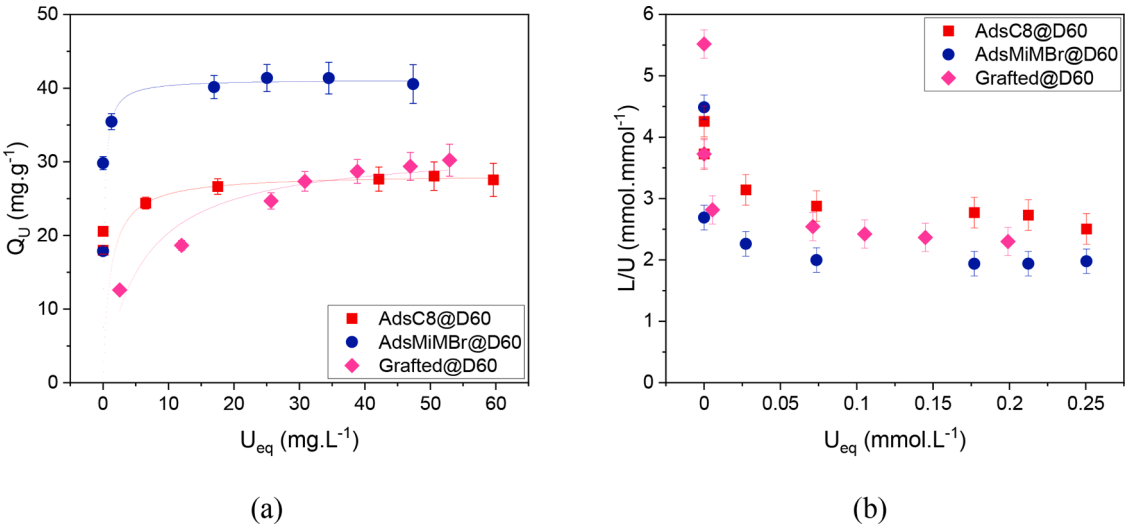

Fig. 6. (a) Uranium extraction isotherms measured for the three studied materials in the low sulfate solution and fits of the data using a Langmuir model. (b) The corresponding ligand/uranium ratios in the three materials.

Table 4
Langmuir modeling of uranium extraction isotherms for the three studied materials.

Solution/Material	Q_{max} (mg•g^{-1})	K_l (L•mg^{-1})	R^2
Low Sulfate Solution			
Grafted@D60	33.78	0.14	0.9895
AdsC8@D60	27.86	2.74	0.9996
AdsMiMBr@D60	40.98	27.11	0.9997
High Sulfate Solution			
Grafted@D60	32.57	0.01	0.9707
AdsC8@D60	36.90	0.19	0.9992
AdsMiMBr@D60	40.65	0.16	0.9994

heterogeneous surface.

Hennig et al.'s data [31] indicate that the disulfate uranyl complex in this solution consists of two sulfate groups in bidentate coordination and a water molecule. The energy required to break these bidentate sulfate-uranyl bonds and form phosphonate-uranyl bonds in the complexation process may explain why the Langmuir constants for the three materials are much lower than in the low sulfate solution (Table 4). In the high sulfate solution, the two impregnated materials have similar Langmuir constants. These results suggest that the limited mobility of the grafted ligand makes it unable in this configuration to adapt to the geometry of the uranyl ions and compete with sulfate complexation due to higher sulfate concentration in this solution.

In the presence of competing ions, both impregnated materials are highly selective for U versus Fe and Mo (Fig. 9) while the grafted material is not. Table 3 shows that the functional groups present on the surface before functionalization with amidophosphonate moieties are

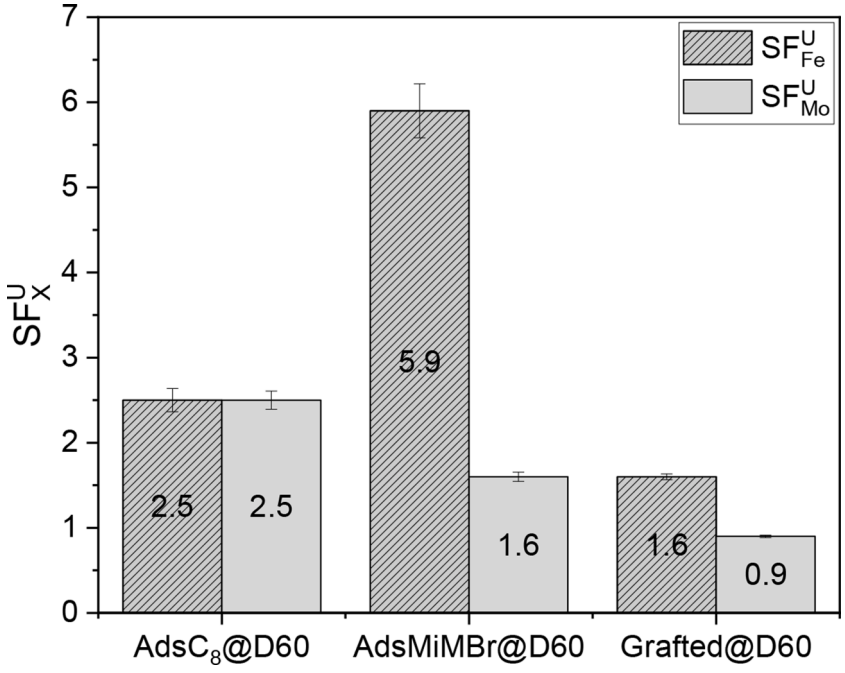

Fig. 7. Selectivity factors for U extraction versus Fe and Mo in the low sulfate solution for the three functionalized silica materials.

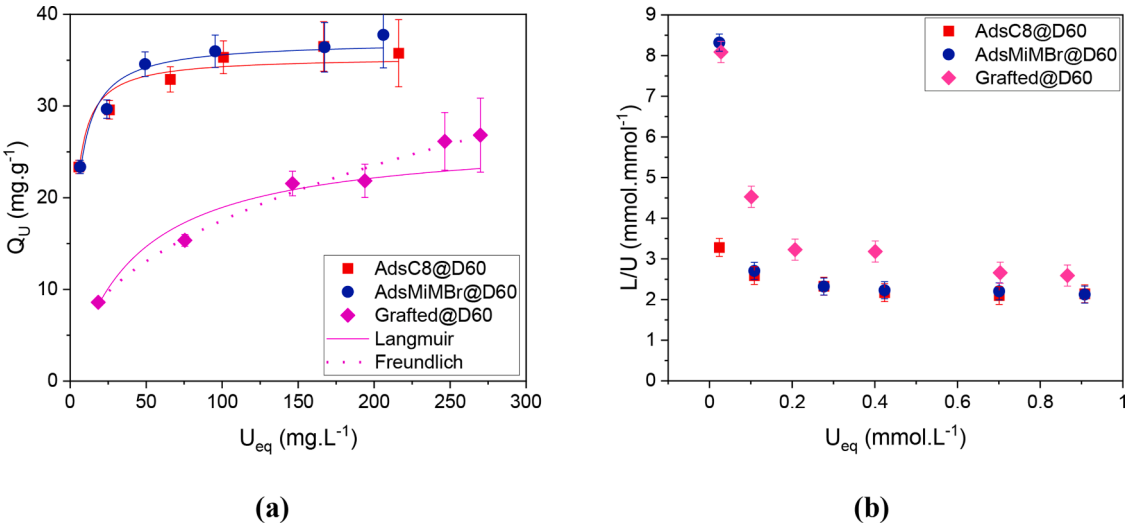

Fig. 8. (a) Uranium extraction isotherms measured for the three studied materials in the high sulfate solution and fits of the data using a Langmuir model. (b) The corresponding ligand/uranium ratios in the three materials.

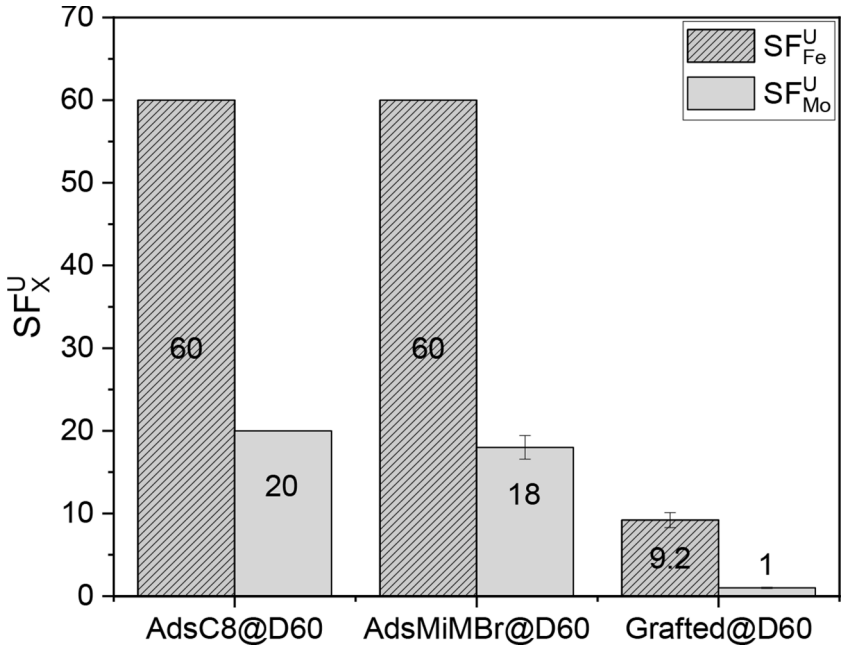

Fig. 9. Selectivity factors for U extraction versus Fe and Mo in the high sulfate solution for the three functionalized silica materials.

not involved either in uranium or in competing cation extraction under these conditions. One of the many possible explanation is that the impregnated ligands might coordinate more easily with the uranium species in solution, probably because their non-covalent attachment affords greater mobility, and are therefore better suited to extract uranium from high sulfate solutions. We thus performed an EXAFS study of the uranium environment under high sulfate conditions to check for differences between the grafted and adsorbed materials.

EXAFS investigations of uranyl extraction

In our previous EXAFS study of the uranium environment of the grafted material under low sulfate conditions [22], we concluded that the amidophophonate moieties bond with U is through a phosphonate group in a monodentate fashion. The first coordination sphere of the uranyl ions is then assumed to be completed by two monodentate sulfate ions and one water molecule. We hypothesized that in a high sulfate medium, the decomplexation energy would be higher because of the energy costs of breaking the sulfate-uranyl bonds and forming phosphonate-uranyl bonds.

To verify this hypothesis (that sulfate-uranyl bonds have to be broken in the high sulfate solution), Uranium L_{III} edge EXAFS spectra were acquired for the initial high sulfate uranium solution, the three intermediate materials and the three amidophosphonate functionalized materials.

The EXAFS spectroscopy data were fitted to evaluate the chemical groups in the material and their interactions. The pseudoradial distribution obtained by Fourier transform of the k-space oscillation between 2.5 and 13.4 Å^{-1} is shown in Fig. 10. The spectra were then fitted in R-space between 1.1 and 5 Å In the extraction conditions used, five different groups (sulfate, silicate, phosphonate, carbonyl and water) can interact either in a mono- or a bidentate fashion with the uranyl inner sphere. The expected distances (from the literature) corresponding to each possible uranyl complex are listed in Table 6.

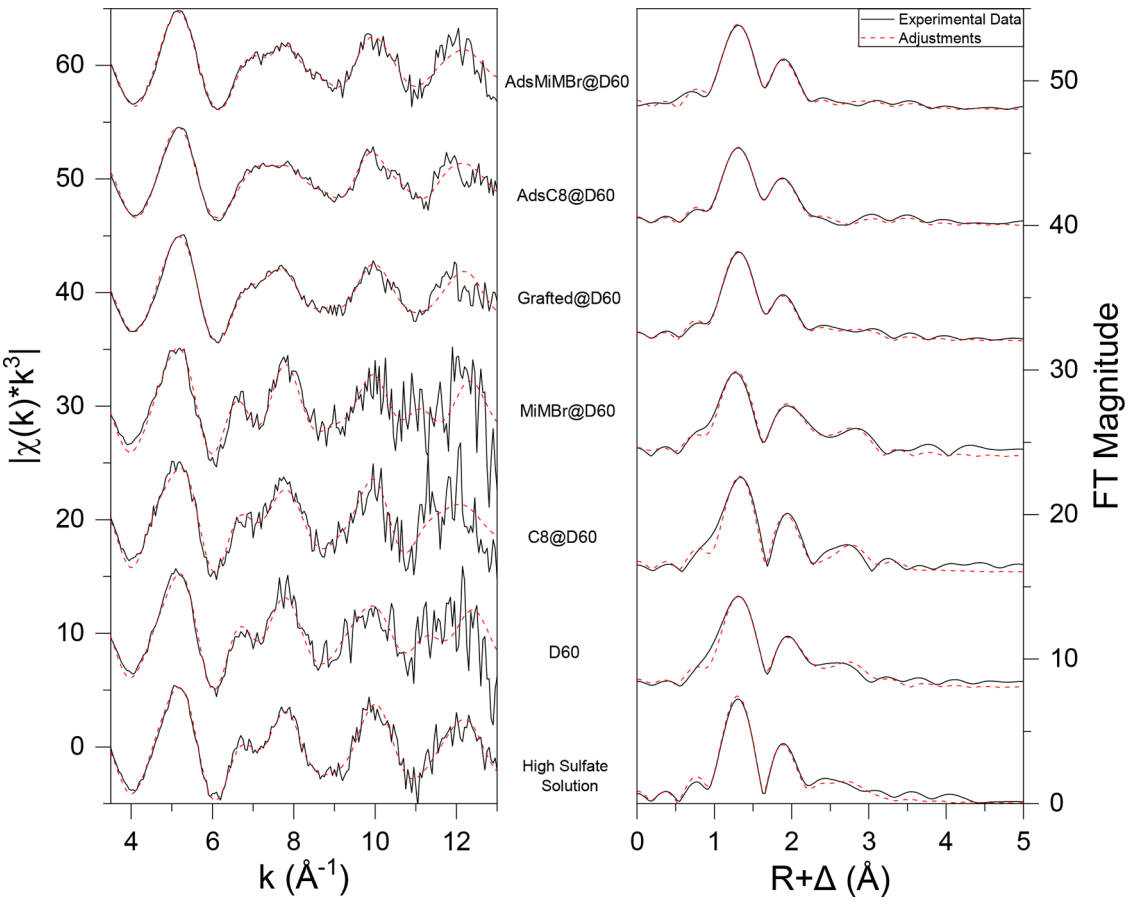

Fig. 10. k^0-weighted Uranium L_{III} edge EXAFS spectra (left) and the corresponding Fourier transforms (right) of the initial high sulfate uranium solution and of the listed samples after contact with this solution. The black and red lines represent the experimental data and the best fits, respectively.

As described previously, [20] the uranium coordination shell must be fitted with two short trans-dioxo oxygen atoms (O_{yl}), because in its oxidation state +VI uranium forms an actinyl ion. In addition, the equatorial uranyl shell can be fitted with two distinct oxygen subshells restricted as a short (2.25–2.45 Å, O_S) and long, (2.45–2.55 Å, O_L) bonds. These ranges were chosen to distinguish between potential coordination groups and because the resolution, inversely related to the maximum wave vector ($\Delta R = \pi/2k_{max}$), limits the EXAFS resolution.

The EXAFS oscillations were recorded between 2.5 and 13.4 $Å^{-1}$ in k-space, allowing bond lengths to be discriminated to within 0.1 Å. To reduce the number of free variables and allow a reliable comparison between coordination numbers, the Debye–Waller factors (σ^2) values were kept fixed at literature values. The O_S and O_L coordination number was left free as well as the second shell L_1 and L_2. In contrast, the O_{yl} coordination value was fixed to 2 and its σ^2 considered as a variable value. The EXAFS parameters obtained from the fits are listed in Table 6.

In the initial solution and the three intermediate materials (without phosphonate ligand), the only heteroatom species considered were sulfates and silicates.

In the initial high sulfate uranium solution, the equatorial plane is best fitted with three to four shorter (O_S) oxygen bonds at 2.36 Å (O_S in Table 6) and two longer (O_L) oxygen bonds at 2.5 Å (O_L in Table 6). This Oxygen splitting can be attributed to the presence of sulfate groups as this involves oxygen bonds different from water molecules (see Table 5). This is confirmed by the second shell fit that provides a more precise description of the uranyl neighborhood (see Table 6). The peak at 3 Å ($R + \varphi$) is attributed to bidentate sulfur atoms in the second shell at 3.13 Å while the absence of any contribution at 3.77 Å indicates that no

Table 5
List of uranyl shell and subshell interactions according to previous reports and the corresponding restrictions for fitting the EXAFS spectra.

	Atom	R (Å)	σ^2 ($Å^2$)	EXAFS Fit restrictions
1st sphere	Silicate O, bidentate [33]	2.26	0.0057	O_S (2.25–2.45 Å) $Å^2 = 0.0045$
	Sulfate O, monodentate [31]	2.27	0.0075	
	Silicate O, monodentate [33]	2.29	0.0035	
	Phosphonate O,monodentate [34]	2.35	0.0024	
	Sulfates O, bidentate [31]	2.40	0.0055	
	Phosphonate O, bidentate [34]	2.50	0.0039	O_L (2.45–2.55 Å) $Å^2 = 0.006$
	Water O [22]	2.49 – 2.55	0.006	
2nd sphere	Silicate Si, bidentate [33]	2.72	0.0034	Si_b
	Phosphonate P, bidentate [35]	3.10	Ø	S_{bi} $Å^2 = 0.006$
	Sulfates S, bidentate [31]	3.11	0.06	
	Silicate Si, monodentate [36]	3.58	Ø	Ø
	Sulfates S, monodentate [22]	3.65–3.67	0.009	S_{mono} $Å^2 = 0.009$
	Phosphonate P, monodentate [34]	3.92	0.0056	P_{mono} $Å^2 = 0.008$

Table 6
Summary of the parameters used to fit the EXAFS spectra of studied materials.

		High sulfate solution	D60	C8@D60	MiMBr @D60	Grafted @D60	AdsC8 @D60	AdsMiMBr @D60
R-factor (%)		1.9	2.6	2.7	3.2	1.1	1.4	0.9
S_0^2		1	1	1	1	0.94	0.77	0.94
ΔE_0 (eV)		2.0	−0.6	6.3	1.2	1.6	2.3	2.9
O_{yle}	CN	2*	2*	2*	2*	2*	2*	2*
	σ^2 (Å^2)	0.0014	0.0028	0.0023	0.0032	0.0025	0.0024	0.0031
	R (Å)	1.76 ± 0.01	1.76 ± 0.01	1.78 ± 0.01	1.75 ± 0.01	1.76 ± 0.01	1.76 ± 0.01	1.76 ± 0.01
O_S	CN	2.9 ± 1	2.3 ± 0.74	3.3 ± 1.2	1.7 ± 0.3	2.9 ± 1	3.2 ± 1.2	2.3 ± 1.3
	σ^2 (Å^2)	0.0055*	0.0055*	0.0055*	0.0055*	0.0055*	0.0055*	0.0055*
	R (Å)	2.36 ± 0.04	2.25 ± 0.03	2.30 ± 0.04	2.28 ± 0.02	2.3 ± 0.05	2.3 ± 0.02	2.32 ± 0.07
O_L	CN	2.2 ± 0.4	4.8 ± 1.4	0.8 ± 1.3	4.6 ± 0.2	2.3 ± 1.5	3.0 ± 1.1	2.0 ± 2.1
	σ^2 (Å^2)	0.0055*	0.0055*	0.0055*	0.0055*	0.0055*	0.0055*	0.0055*
	R (Å)	2.5 ± 0.06	2.44 ± 0.02	2.6 ± 0.2	2.46 ± 0.01	2.45 ± 0.06	2.44 ± 0.03	2.44 ± 0.08
L1	CN	1.8 ± 0.4	2.2 ± 0.5	1.8 ± 0.8	2.6 ± 0.4	1.0 ± 0.4	0.5 ± 0.3	0.4 ± 0.3
	σ^2 (Å^2)	0.0060*	0.0060*	0.0060*	0.0060*	0.0060*	0.0060*	0.0060*
	R (Å)	3.13 ± 0.02	3.11 ± 0.02	3.15 ± 0.03	3.15 ± 0.01	3.14 ± 0.03	3.24 ± 0.06	3.14 ± 0.05
L2	CN	0	1.2 ± 1	1.4 ± 1.7	0.5 ± 1	0.5 ± 0.5	1.7 ± 0.9	1.5 ± 0.7
	σ^2 (Å^2)	0.0090*	0.0090*	0.0090*	0.0090*	0.0090*	0.0090*	0.0090*
	R (Å)	3.77 ± 0.06	3.67 ± 0.07	3.76 ± 0.09	3.76 ± 0.06	3.89 ± 0.12	3.86 ± 0.04	3.91 ± 0.04

CN, Coordination number.
* fixed values, σ^2: Debye-Waller factor; R, uranium-atom distance.

monodentate sulfate is detected. In short, the EXAFS data for the high sulfate solution are consistent with a uranyl equatorial plane consisting of almost two bidentate sulfate groups completed by water molecule. This results agrees well with previous measurements in similar condition by Hennig [31].

In the C8@D60 samples, the oxygen shell is similar to the one observed for the initial uranium solution but with slightly more short oxygen atoms but much less long. This overall short U-Oeq distances is consistent with the lower average coordination number compared to the initial solution. In the second coordination sphere, the L_1 shell distance and coordination number is still consistent with bidentate sulfate groups whereas a small amount of L_2 is detected corresponding to monodentate sulfate groups. This is consistent with the hydrophobic nature of the octyl chains found on the surface of C8@D60, suggesting that uranium-disulfate may be destabilized by these octyl chains.

In the D60 and MiMBr@D60 samples, the equatorial plane is best fitted with the two types of bonded oxygen atoms in the first shell reaching a minimum values, with bond lengths either close to 2.25 Å (O_S in Table 6), attributed to monodentate sulfate groups (Table 5), and with bond lengths close to 2.44 Å (O_L in Table 6), attributed to bidentate interactions with sulfate groups. Looking further at the second shell confirms this interpretation: the peak at 3 Å ($R + \varphi$) is best modeled by bidentate sulfur atoms in the second shell at 3.13 Å, while the peak at 3.67 Å can be assigned to monodentate sulfur atoms. In both cases (in the D60 and MiMBr@D60 materials), the uranyl atom appears to be surrounded by close to two bidentate sulfate groups and monodentate sulfates. This is consistent with the hydrophilic functions on the surface of D60 and MiMBr@D60, respectively siloxane and methylimidazolium, suggesting that uranium may lies within these chains as anionic uranyl tetrasulfate.

To summarize, in all samples without phosphonate ligands, the uranyl ions appear to be surrounded by bidentate sulfate groups. In the high sulfate solution, the coordination sphere is completed by at least one water molecule, except in the C8@D60 sample and monodentate sulfate in the MiMBr@D60 material and in D60 which appear to be in the vicinity of the uranyl ions.

For the three amidophosphonate-functionalized samples, the second coordination sphere become more difficult to read. Heteroatoms (P, S and Si) from sulfates, silicates and phosphonates results into similar second shell distances and the fits interpretation depends on both coordination shell interrelation. In all three cases, the equatorial plane is best fitted with two types of bonded oxygen atoms at 2.3 Å, consistent with monodentate sulfate or phosphonate, and at 2.45 Å, consistent with bidentate sulfate and possibly bidentate phosphonates. The results obtained for the materials without phosphonate ligands unambiguously indicate that bidentate sulfate groups are the predominant coordination mode of sulfate in the system. In grafted and adsorbed materials, both the 2.45 Å interactions (O_L in Table 6) and the U-L_1 at 3.15 Å assigned to bidentate moieties, decrease. In the second shell, the L1 coordination number decreases from about 2 for materials without phosphonate to 1 and 0.5 for the grafted and adsorbed samples respectively. Both results (first and second coordination sphere) indicate a decrease in the bidentate sulfate coordination mode, higher for adsorbed samples than for the grafted one. Concomitantly the longer U-L_2 bond length at 3.86–3.91 as well as the short O_S 2.30 Å increase. This lenght increases consistently while the amount of bidentate sulfate ligands decrease, and this U-L_2 bonds is too large to be attributed a monodentate sulfate (U-S_{mono} is expected at 3.75 Å whereas the measured UL_2 is 3.9 Å). This signal can thus be assigned to monodentate phosphonate atoms. Altogether, these results are consistent with a substitution of bidentate sulfate ligands by phosphonate groups in all three samples. Moreover it states that this effect is twice more pronounced for the adsorbed samples in comparison to the grafted one. Although the species making up the first coordination sphere of uranyl cannot be firmly identified, the second sphere seems to be consistent with the results of the extraction experiments and the formation of 1:2 U/L complexes.

Indeed, the fact that in both impregnated materials, the peak at 3.86–3.91 Å can be attributed to two monophosphonate groups is consistent with the ligand/uranium ratio in the absence of competing ions, confirming that two amidophosphonate moieties are required to complex uranyl. The peak at 3.14 Å attributed to bidentate sulfates has a coordination of 0.5, while the coordination number in the initial solution is 2, indicating that the number of bisulfate ions around uranyl falls drastically as the latter interact with the impregnated materials.

In the grafted material in contrast, the peak at 3.89 Å can be attributed to 0 or at most 1 monophosphonate group while the bidentate sulfate peak at 3.14 Å accounts at least for 1. This is consistent with the grafted material being outcompeted for uranyl by the bidentate sulfate groups found in this high sulfate solution.

As suggested above, the EXAFS analysis confirms that uranium complexation by phosphonate groups requires the breaking of bidentate sulfate-uranyl bonds and formation of phosphonate-uranyl bonds. The EXAFS data are also consistent with the interpretation that this process is less likely to occur in the grafted materials than in the impregnated materials because the energy barrier in the case of the (less mobile) grafted ligands is higher than for the impregnated ligands.

Conclusion

This study shows how the functionalization method used to prepare extraction materials can affect the uranium extraction mechanism and the extraction efficiency. Various functionalized silica materials were investigated as uranium extractants in two sulfuric acid solutions with and without Fe and Mo as competing cations: a low sulfate solution, and a high sulfate solution. Silica supports were functionalized with amidophosphonate moieties either by peptide grafting or by impregnation after different surface modifications.

Our results show that both types of material had good extraction efficiency and selectivity in the low sulfate solution. In the high sulfate solution, the impregnated materials extracted uranium more efficiently and more selectively with respect to Fe and Mo than the grafted material did, whose extraction capacity was much lower at the higher sulfate concentration. EXAFS data support the interpretation that the grafted functional groups compete poorly for uranium with the bidentate sulfates found in the high sulfate solution, in contrast with the impregnated ones, with two amidophosphonate moieties required to extract one uranyl ion, the same ratio as observed in the low sulfate solution. These observations suggest that the bidentate sulfate-uranyl bonds (in solution) are replaced by phosphonate-uranyl bonds with the ligands present on the surface of the pores in the materials. Impregnation affords more flexibility to the ligands than grafting does, and thus reduces the energy required for desulfurization. This may explain the higher extraction capacity and selectivity of the impregnated materials. Impregnated materials seem therefore to be the best candidates to extract uranium from high sulfate solutions. Their ability to be fully recycled, eluted and reused is currently being studied.

Declaration of Competing Interest

There are no conflicts of interest to declare.

Acknowledgments

This work was supported by the French Alternative Energies and Atomic Energy Commission, and the NOPRA Project. The authors also thank Rajae Fakiri for assistance with organic synthesis and on the characterization of organic compounds and Dr Fabio Ziarelli (Spectropole Aix-Marseille University) for performing the CP/MAS NMR experiments. The authors gratefully acknowledge Pier Lorenzo Solari for the experimental support on MARS beamline. Soleil Synchrotron is acknowledged for providing beamtimes.

Supplementary materials

Supplementary material associated with this article can be found, in the online version, at doi:10.1016/j.ceja.2021.100225.

References

[1] J. Veliscek-Carolan, K.A. Jolliffe, T.L. Hanley, Selective sorption of actinides by titania nanoparticles covalently functionalized with simple organic ligands, ACS Appl. Mater. Interfaces 5 (2013) 11984–11994.
[2] P.J. Lebed, J.D. Savoie, J. Florek, F. Bilodeau, D. Lariviere, F. Kleitz, Large pore mesostructured organosilica-phosphonate hybrids as highly efficient and regenerable sorbents for uranium sequestration, Chem. Mater. 24 (2012) 4166–4176.
[3] J. Florek, F. Chalifour, F. Bilodeau, D. Larivière, F. Kleitz, Nanostructured hybrid materials for the selective recovery and enrichment of rare earth elements, Adv. Funct. Mater. 24 (2014) 2668–2676.
[4] J.L. Vivero-Escoto, M. Carboni, C.W. Abney, K.E. deKrafft, W. Lin, Organo-functionalized mesoporous silicas for efficient uranium extraction, Microporous Mesoporous Mater. 180 (2013) 22–31.
[5] A.K.S. Deb, P. Ilaiyaraja, D. Ponraju, B. Venkatraman, Diglycolamide functionalized multi-walled carbon nanotubes for removal of uranium from aqueous solution by adsorption, J. Radioanal. Nucl. Chem. 291 (2012) 877–883.
[6] Z. Dai, Y. Sun, H. Zhang, D. Ding, L. Li, Highly efficient removal of uranium(VI) from wastewater by polyamidoxime/polyethyleneimine magnetic graphene oxide, J. Chem. Eng. Data 64 (2019) 5797–5805.
[7] M. Carboni, C.W. Abney, K.M.L. Taylor-Pashow, J.L. Vivero-Escoto, W. Lin, Uranium sorption with functionalized mesoporous carbon materials, Ind. Eng. Chem. Res. 52 (2013) 15187–15197.
[8] C. Siva Kesava Raju, M.S. Subramanian, Sequential separation of lanthanides, thorium and uranium using novel solid phase extraction method from high acidic nuclear wastes, J. Hazard. Mater. 145 (2007) 315–322.
[9] M. Zhang, Y. Li, C. Bai, X. Guo, J. Han, S. Hu, H. Jiang, W. Tan, S. Li, L. Ma, Synthesis of microporous covalent phosphazene-based frameworks for selective separation of uranium in highly acidic media based on size-matching effect, ACS Appl. Mater. Interfaces 10 (2018) 28936–28947.
[10] J. Yu, L. Yuan, S. Wang, J. Lan, L. Zheng, C. Xu, J. Chen, L. Wang, Z. Huang, W. Tao, Z. Liu, Z. Chai, K.John Gibson, W. Shi, Phosphonate-decorated covalent organic frameworks for actinide extraction: a breakthrough under highly acidic conditions, CCS Chem. 1 (2021) 286–295.
[11] J. Lei, H. Liu, F. Wen, X. Jiang, C. Yuan, Q. Chen, J. Liu, X. Cui, F. Yang, W. Zhu, R. He, Tellurium nanowires wrapped by surface oxidized tin disulfide nanosheets achieves efficient photocatalytic reduction of U(VI), Chem. Eng. J. 426 (2021), 130756.
[12] J. Lei, H. Liu, C. Yuan, Q. Chen, J. Liu, F. Wen, X. Jiang, W. Deng, X. Cui, T. Duan, W. Zhu, R. He, Enhanced photoreduction of U(VI) on WO3 nanosheets by oxygen defect engineering, Chem. Eng. J. 416 (2021), 129164.
[13] G. Arrachart, N. Aychet, G. Bernier, F. Burdet, A. Leydier, M. Miguirditchian, S. Pellet-Rostaing, G. Plancque, R. Turgis, E. Zekri, New Bifunctional Carbamoylphosphonates As Extractants For uranium(VI) and a Process For Preparation Thereof, AREVA Mines, 2013, p. 72. Fr.
[14] D.K. Singh, S. Mondal, J.K. Chakravartty, Recovery of uranium from phosphoric acid: a review, Solvent Extr. Ion Exch. 34 (2016) 201–225.
[15] P. Baron, G. Bernier, D. Hartmann, C. Laluc, M. Marbet, Use of Compounds With Amide and Phosphonate Groups to Extract Uranium(Vi) From Sulfuric Uranium-Bearing Ore Leaching Soln, AREVA Mines, 2014, p. 35. Fr.
[16] R. Turgis, A. Leydier, G. Arrachart, F. Burdet, S. Dourdain, G. Bernier, M. Miguirditchian, S. Pellet-Rostaing, Carbamoylalkylphosphonates for dramatic enhancement of uranium extraction from phosphates ores, Solvent Extr. Ion Exch. 32 (2014) 685–702.
[17] G.S. Conary, R.L. Meline, R. Schaeffer, E.N. Duesler, R.T. Paine, Synthesis and coordination chemistry of trifunctional phosphono-bis-carbonyl alkane ligands, Inorg. Chem. Acta 201 (1992) 165–176.
[18] T.H. Siddall, Bidentate organophosphorus compounds as extractants, J. Inorg. Nucl. Chem. 25 (1963) 883–892.
[19] R. Turgis, A. Leydier, G. Arrachart, F. Burdet, S. Dourdain, G. Bernier, M. Miguirditchian, S. Pellet-Rostaing, Uranium extraction from phosphoric acid using bifunctional amido-phosphonic acid ligands, Solvent Extr. Ion Exch. 32 (2014) 478–491.
[20] A. Charlot, F. Cuer, A. Grandjean, The effect of pore diameter in the arrangement of chelating species grafted onto silica surfaces with application to uranium extraction, New J. Chem. 41 (2017) 503–511.
[21] L. Fryxell, Birnbaum Fiskum, hong Wu, Actinide sequestration using self-assembled monolayers on mesoporous supports, Environ. Sci. Technol. 39 (2005) 1324–1331.
[22] A. Charlot, T. Dumas, P.L. Solari, F. Cuer, A. Grandjean, A spectroscopic study of uranium and molybdenum complexation within the pore channels of hybrid mesoporous silica, Eur. J. Inorg. Chem. 2017 (2017) 563–573.
[23] S. Dourdain, I. Hofmeister, O. Pecheur, J.F. Dufreche, R. Turgis, A. Leydier, J. Jestin, F. Testard, S. Pellet-Rostaing, T. Zemb, Synergism by coassembly at the origin of ion selectivity in liquid-liquid extraction, Langmuir ACS J. Surf. Colloids 28 (2012) 11319–11328.
[24] T.Le Nedelec, A. Charlot, F. Calard, F. Cuer, A. Leydier, A. Grandjean, Uranium adsorption from sulfuric acid media using silica materials functionalised with amide and phosphorous ligands, New J. Chem. 42 (2018) 14300–14307.
[25] M. Li, P.J. Pham, T. Wang, C.U. Pittman, T. Li, Selective extraction and enrichment of polyunsaturated fatty acid methyl esters from fish oil by novel π-complexing sorbents, Sep. Purif. Technol. 66 (2009) 1–8.
[26] R. Kore, R. Srivastava, Synthesis of triethoxysilane imidazolium based ionic liquids and their application in the preparation of mesoporous ZSM-5, Catal. Commun. 18 (2012) 11–15.
[27] A. Charlot, S.E. Mourabit, F. Goettmann, G. Arrachart, R. Turgis, A. Grandjean, From phosphate rocks to uranium raw materials: hybrid materials designed for selective separation of uranium from phosphoric acid, RSC Adv. 4 (2014) 64138–64141.
[28] B. Ravel, M. Newville, ARTEMIS ATHENA, HEPHAESTUS: data analysis for X-ray absorption spectroscopy using IFEFFIT, J. Synchrotron Radiat. 12 (2005) 537–541.
[29] J.J. Rehr, R.C. Albers, Theoretical approaches to X-ray absorption fine structure, Rev. Mod. Phys. 72 (2000) 621–654.
[30] M. Magi, E. Lippmaa, A. Samoson, G. Engelhardt, A.R. Grimmer, Solid-state high-resolution silicon-29 chemical shifts in silicates, J. Phys. Chem. 88 (1984) 1518–1522.
[31] K.S. Christoph Hennig, Vinzenz Brendler, Henry Moll, Satoru Tsushima, Andreas C. Scheinost, EXAFS Ivestigation of U(VI), U(IV), and Th(IV) sulfato complexes in aqueous solution, Inorg. Chem. 46 (2007) 5882–5892.
[32] T. Vercouter, P. Vitorge, B. Amekraz, C. Moulin, Stoichiometries and thermodynamic stabilities for aqueous sulfate complexes of U(VI), Inorg. Chem. 47 (2008) 2180–2189.
[33] H.M.T. Reicha, T. Arnold, M.A. Denecke, C. Hennig, G. Geipel, G. Bernhard, P.G.A. H. Nitsche, J.J. Bucher, N.M. Edelstein, D.K. Shuh, An EXAFS study of uranium(VI)

sorption onto silica gel and ferrihydrite, J Electron Spectrosc. Relat. Phenom. 96 (1998) 237–243.
[34] O. Pecheur, D. Guillaumont, S. Dourdain, L. Berthon, R. Turgis, C. Fillaux, G. Arrachart, F. Testard, Uranium extraction by a bifunctional amido-phosphonic acid: coordination structure and aggregation, Solvent Extr. Ion Exch. (2016) 1–14.
[35] J.D. Kubicki, G.P. Halada, P. Jha, B.L. Phillips, Quantum mechanical calculation of aqueuous uranium complexes: carbonate, phosphate, organic and biomolecular species, Chem. Cent. J. 3 (2009) 10.
[36] V. Wheaton, D. Majumdar, K. Balasubramanian, L. Chauffe, P.G. Allen, A comparative theoretical study of uranyl silicate complexes, Chem. Phys. Lett. 371 (2003) 349–359.